Analysis of azimuthal-angle scans in resonant x-ray Bragg diffraction and parity even and odd atomic multipoles in the multiferroic modification of the terbium manganate $TbMnO_3$

V. Scagnoli*
European Synchrotron Radiation Facility, BP 220, 38043 Grenoble Cedex 9, France

S. W. Lovesey
ISIS Facility, RAL, Oxfordshire OX11 0QX, United Kingdom
and Diamond Light Source Ltd., Oxfordshire OX11 0QX, United Kingdom
(Received 9 September 2008; published 15 January 2009)

We present a theoretical analysis of resonant x-ray Bragg diffraction data from multiferroic $TbMnO_3$ presented by Mannix *et al.* [Phys. Rev. B **76**, 184420 (2007)] and Voigt *et al.* [Phys. Rev. B **76**, 104431 (2007)]. We have chosen an approach that does not rely on knowledge of the low-temperature phase space group of the sample, which is not precisely known. Results show that the low-temperature satellite reflections originate from dipole-dipole (E1-E1) and dipole-quadrupole (E1-E2) events. Presence on quadrupole-quadrupole (E2-E2) events can be excluded. The physical origin of the data is discussed in terms of atomic multipoles (expectation value of an operator equivalent) that represent magnetization, lattice distortions, and magnetoelectric properties of the Tb and Mn ions. A handed (chiral) cycloid of atomic multipoles, traced out in the *b*-*c* plane, is shown to be a plausible model of the Tb electron structure within a multiferroic modification that exists in the temperature interval $7\ \mathrm{K} < T < 28\ \mathrm{K}$. Appendixes A–F record universal expressions for unit-cell structure factors appropriate to all four polarization channels (σ'-σ, σ'-π, π'-σ, π'-π) of E1-E1, E1-E2, and E2-E2 resonance events.

DOI: 10.1103/PhysRevB.79.035111 PACS number(s): 78.70.Ck, 71.30.+h

I. INTRODUCTION

X-ray Bragg diffraction by a crystal with signal enhancement by an atomic resonance was demonstrated many years ago. Seminal observations of this diffraction came from Templeton and Templeton[1] and Finkelstein *et al.*,[2] with timely theoretical analyses by Dmitrienko[3] and Carra and Thole.[4] In 2005, Dmitrienko *et al.*[5] made a survey of experiments utilizing resonant diffraction while Lovesey *et al.*[6] and Collins *et al.*[7] shaped theoretical concepts in x-ray diffraction and absorption by nonmagnetic and magnetic materials at more or less the same time. The main attractions of resonant x-ray diffraction include the precision inherent in Bragg diffraction imposed by symmetry-based selection (extinction) rules, selection of an ion type from tuning the primary energy to a specific atomic resonance, and additional detail to be found in the amplitudes for rotated states of polarization. Information on electron charge, orbital, and spin degrees of freedom derived from resonant Bragg diffraction is not available from any other experimental method.

Angular anisotropy in valence electron states associated with the resonant ion is mirrored in the variation in the Bragg intensity with the setting of the crystal. Rotation of the crystal around the Bragg wave vector in an experiment is referred to as an azimuthal-angle scan.[2,8] Intensity of a Bragg reflection as a function of the azimuthal angle is a direct measure of the angular properties of the environment of the resonant ion by virtue of Neumann's principle. In other words, information on the point group from an azimuthal-angle scan complements information about the space group derived from Bragg intensities. The complementary information assumes great significance when modification of the material's properties is visible only in a few Bragg reflections, which are insufficient in assisting in additional structure refinement. In such cases, one is deprived of complete structural information as a firm basis in a quest for insight to various electronic phenomena at an atomic level of detail, e.g., optical activity, ferroelectricity, magnetoelectricity, and magnetic motifs. One such case is the enigmatic phase IV of CeB_6 doped with La.[9]

A successful analysis of diffraction data given in Ref. 9 was achieved by confronting calculated structure factors with data gathered in azimuthal-angle scans. In the present work, we extend this mode of attack by calculating universal forms of structure factors as functions of the azimuthal angle for E1-E1, E1-E2, and E2-E2 resonance events. The foundation of our work is covered in Refs. 6 and 7. Results for unit-cell structure factors derived here are exploited in a thorough analysis of data published for multiferroic terbium manganate.

The Secs. II and III of our paper are devoted to terbium manganate and its multiferroic modification. Particular emphasis is posed on the relationship between the observed diffracted intensities and their correspondence to atomic multipoles. Section IV contains our conclusions. In Appendixes A and B we first summarize key features of atomic multipoles observed in diffraction and record a generic unit-cell structure factor. The latter is then re-expressed to form universal quantities that are listed in Appendixes C–E.

II. ELECTRIC AND MAGNETIC PROPERTIES OF $TbMnO_3$

At room temperature terbium manganate has no electronic properties of special interest. It possesses an orthorhombic perovskite structure usually described in terms of the space-group *Pbnm* (standard setting *Pnma*, No. 62) in which cat-

ions use Wyckoff positions 4*b* (Mn) and 4*c* (Tb) (Table IV of Ref. 10). Cell parameters are $a=5.3090(5)$ Å, $b=5.8118(5)$ Å, and $c=7.3860(7)$ Å.[10] In this structure, manganese Mn^{3+} ($3d^4$, $S=2$) ions are enclosed by oxygen ions. However, surrounding octahedra are not rigid and octahedral-site distortion may bias orbital ordering and spin ordering.[11] The environment at position 4*b* is simply a center of inversion symmetry and devoid of any other symmetry. By contrast, tripositive terbium ions occupy cavities in the chemical structure. The environment at position 4*c* has mirror symmetry, *m*, with a diad axis of rotation parallel to the crystal *c* axis. Absence of a center of symmetry at positions used by Tb^{3+} ions allows parity-odd resonance events, of which E1-E2 (treated in Appendix D) is an example.

In an interval of temperature 28 K$<T<$41 K, which we call phase (i), magnetization exists on the Mn sublattice which is collinear, polarized along the *b* axis, and incommensurate with a wave vector $\mathbf{q}\sim 0.28\mathbf{b}^*$ while Tb ions are not ordered. The long-range magnetic order is accompanied by modulation of the Mn sublattice with sinusoidal displacements along the *c* axis.

Within the range 7 K$<T<$28 K, called phase (ii), modifications create a multiferroic state. The spatially varying electric-dipole moment associated with Mn displacements undergoes a first-order transition to a ferroelectric phase, leaving a spontaneous polarization along the *c* axis. Simultaneously, magnetization on the Mn sublattice becomes noncollinear with a component along the *c* axis. Terbium moments in phase (ii) display noncollinear order, with transverse polarization along the *a* axis and wave vector **q**. The observation of a magnetically controlled ferroelectric polarization demonstrates a giant magnetoelectric effect.[12]

Below 7 K, labeled phase (iii), Tb moments adopt the same configuration as in phase (ii) but the wave vector is distinctly different, namely, $\mathbf{q}'\sim 0.42\mathbf{b}^*$.

At present, there is no consensus on all details of the various configurations of magnetic moments in terbium manganate[10,13–18] but a critical review of published work is not undertaken. The lack of consensus might reflect sensitivity of the magnetic configurations to sample preparation. Magnetoelectric correlations in terbium manganate are reviewed by Fiebig.[19] Let us note that a magnetic structure incommensurate with the chemical structure heralds a loss of inversion symmetry. Whether the incommensurate structure is driven by a lattice distortion, a first-order effect, or magnetic order, a second-order effect, remains to be settled. In the multiferroic modification, the crystal structure is likely to be close to the room-temperature chemical structure simply because the polar moment is relatively small.

III. ANALYSIS OF DATA ON $TbMnO_3$

In this section we analyze various azimuthal-angle scans reported for terbium manganate by Mannix *et al.*[20] The reflections we discuss have crystal *a* and *b* axes in the plane of scattering, and for an azimuthal angle $\psi=0°$, the *c* axis is normal to the plane. Our choice of origin coincides with the one used by Voigt *et al.*[21] and it differs by $\psi=90°$ from the one used by Mannix *et al.*,[20] as illustrated in Fig. 2. Also,

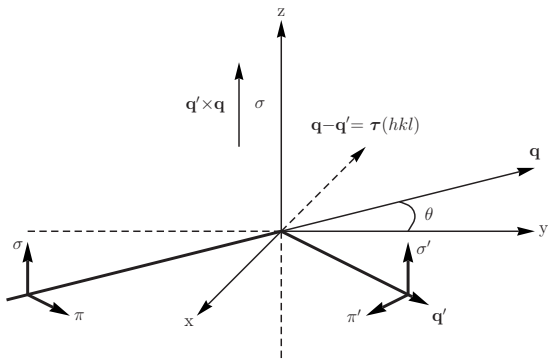

FIG. 1. The diagram illustrates the Cartesian coordinate system (x,y,z) adopted for Bragg diffraction and the relation to states of polarization in the primary (σ,π) and secondary (σ',π') beams of x rays. The primary beam is deflected through an angle 2θ and $\tau(h,k,l)$ is the Bragg wave vector for the reflection labeled by Miller indices h,k,l.

referring to Fig. 1 our secondary states of polarization are denoted by a prime σ' and π' while primary states are unprimed σ and π.[6,7]

A unit-cell structure factor is denoted by $F_{\mu\nu}$, where μ and ν label states of polarization; it is commonplace to use σ polarization normal to the plane of scattering and π polarization parallel to the plane as illustrated in Fig. 1. The generic form of $F_{\mu\nu}$ is

$$F_{\mu\nu}=\sum_K \boldsymbol{J}^K_{\mu\nu}\cdot\boldsymbol{D}^K\cdot\Psi^K, \tag{1}$$

where the spherical tensor $\boldsymbol{J}^K_{\mu\nu}$ describes states of the primary and secondary x rays. Later we consider E1-E1, E1-E2, and E2-E2 resonance events and there is a different $\boldsymbol{J}^K_{\mu\nu}$ for each event.[6] The quantity $\boldsymbol{D}^K$ in Eq. (1) is a rotation matrix used to orientate the crystal in right-handed Cartesian coordinates (x,y,z) that describe the scattering geometry, and the coordinates are illustrated in Fig. 1. As before,[6,7] we choose **z** parallel to σ polarization, normal to the plane of scattering, and **x** antiparallel to the Bragg wave vector, labeled $\tau(h,k,l)$ where *h*, *k*, and *l* are Miller indices. The rotation matrix is a function of the azimuthal angle ψ that measures rotation of the crystal around the Bragg wave vector. Ψ^K is given by

$$\Psi^K_Q=\sum_d e^{i\mathbf{d}\cdot\boldsymbol{\tau}}\langle T^K_Q\rangle_d, \tag{2}$$

where $\langle T^K_Q\rangle_d$ is a multipole which represents the electronic origin of the scattering. The positive integer *K* is the rank of the multipole, and the projection *Q* [omitted in Eq. (1) for clarity] can take the $(2K+1)$ integer values which satisfy $-K\leq Q\leq K$. For a dipole transition, multipoles up to rank 2 contribute $(K\leq 2)$. $K=0$ reflects charge contribution, $K=1$ reflects time-odd dipole, and $K=2$ reflects time-even quadrupole (so-called Templeton and Templeton scattering or anisotropy of the tensor of susceptibility). Only parity-even multipoles arise in the case of dipole E1-E1 and E2-E2 transitions. They possess the property of a one-to-one correspondence between rank, *K*, and symmetry with respect to time reversal. We add the superscript *t* (*u* and *g*) in $\Psi^{t,K}_Q$ to

denote the fact that is a sum of parity-even (parity-odd, time-even, and time-odd, respectively) multipoles.

Given knowledge of the space group, one can construct unit-cell structure factors, and several examples are listed in Ref. 6. In the absence of this knowledge it pays dividends to write Ψ_Q^K, written in the coordinate space (x,y,z), as a sum of quantities that are even (A_Q^K) and odd (B_Q^K) functions of the projection Q with $-K \leq Q \leq K$. The structure factor so defined is a universal quantity that is listed in Appendixes C–E for all $\boldsymbol{A}^K$ and $\boldsymbol{B}^K$. Results for $F_{\mu\nu}$ reported therein have been derived in two independent calculations and crosschecked for absolute accuracy. Dependence of the structure factor on the actual Bragg wave vector $\tau(h,k,l)$, and properties of the crystal, is kept in $\boldsymbol{A}^K$ and $\boldsymbol{B}^K$. Appendixes C–E cover E1-E1, E1-E2, and E2-E2 resonance events, respectively. Corresponding results for the E1-M1 event, discussed in Refs. 7 and 22, are easy to construct.

A. Phase (ii): (3,0,0) reflection at the Tb L_3 edge

In phase (ii), Mannix *et al.*[20] report intensity in the rotated π'-σ channel of diffraction at the space-group forbidden reflection (3,0,0) with signal enhancement by the Tb L_3 edge. As a function of azimuthal angle, intensity appears to follow a $\sin^2\psi$ dependence.

Following Mannix *et al.*,[20] the intensity is assigned to an E1-E1 event. From an inspection of Eq. (C2) a pure $\sin^2\psi$ dependence of the intensity may be generated by multipoles in $A_{1,0}^t$ or $B_{2,2}^t$, where $A_{1,0}^t$ is dipolar magnetization, and $B_{2,2}^t$ is Templeton and Templeton scattering by a charge quadrupole. Diffraction by a motif of quadrupoles (such a contribution to diffraction is said to arise from orbital ordering) permitted in the room-temperature structure is entirely plausible since, according to the structure factor (A2) for Tb ions in the space-group *Pbnm*, $B_{2,2}^t$ is allowed to be different from zero. Even though at 11 K a component of the Mn sublattice magnetization is parallel to the c axis, the configuration is believed to be cycloidal which will not induce a component in the Tb magnetization that is solely parallel to the c axis. An induced component of Tb magnetization parallel to the a axis could allow $B_{1,1}^t$ to be different from zero and that such a contribution is in the E1-E1 amplitude for polarization π'-σ. This particular contribution to the π'-σ amplitude is independent of ψ and, if present in the π'-σ diffraction amplitude, it will prevent the intensity from being zero at $\psi=0°$ which is not a conclusion supported by available data.[20]

Thus data in an azimuthal-angle scan at (3,0,0) collected in phase (ii) are consistent with Templeton and Templeton scattering, which is permitted in *Pbnm*, and Tb magnetization along b and c directions.

B. *F*-type reflections

Below 41 K, so-called *F*-type satellite reflections $(0,k\pm q,0)$ with even integer k are found at both the Mn K edge and the Tb L_3 edge. Diffraction is predominantly in the π'-σ channel and intensities follow a $\sin^2\psi$ dependence. As already noted before, a pure $\sin^2\psi$ dependence of the intensity in an E1-E1 event may be generated by multipoles in $A_{1,0}^t$ or $B_{2,2}^t$, where $A_{1,0}^t$ is dipolar magnetization, and $B_{2,2}^t$ is Templeton and Templeton scattering by a motif of charge quadrupoles that is permitted in *Pbnm* for diffraction by both Mn, with Miller index $l=0$, and Tb. If these are the only contributions different from zero, there is no diffraction in the σ'-σ channel, as required by the data gathered at the Mn K edge.[20]

This picture is adequate to describe observations at the Mn K edge. On the other hand, at the Tb L_3 edge intensity as a function of ψ does not vanish. Instead, there appears to be constant contribution which grows with decreasing temperature. Such a constant contribution is created by a configuration of magnetic dipoles that makes $B_{1,1}^t$ different from zero ($B_{1,1}^t$ is not found in the σ'-σ channel). If the observed intensity at the Tb L_3 edge is purely magnetic in origin, the configuration of dipole moments must have both $A_{1,0}^t$ and $B_{1,1}^t$ different from zero. In contrast, absence of a constant contribution to azimuthal-angle scans at the Mn K edge implies that for the Mn magnetization and *F*-type reflections, $B_{1,1}^t=0$. Regarding the relation of $A_{1,0}^t$ and $B_{1,1}^t$ to components of Tb magnetization, note that, according to Eq. (B5), for reflections $(0,k,0)$ with correspondence between angular components of Ψ_Q^K and angular components of electronic structure, $B_{1,1}^t$ is proportional to magnetization along b and $A_{1,0}^t$ is proportional to magnetization along c.

Voigt *et al.*[21] reported azimuthal-angle data collected on an *F*-type satellite reflection, with the primary energy tuned to the Tb L_2 edge, and the sample held at a temperature of 6 K, namely, phase (iii). These data and corresponding data reported by Mannix *et al.*[20] are at one on the shape of intensity as a function of ψ, including a constant contribution.

C. *C*-type reflections at the Tb L_3 edge

Resonant satellites $(0,k\pm q,0)$ with odd integer k appear at the Tb L_3 edge on taking the sample below 28 K. These so-called *C*-type reflections herald phase (ii), with magnetoelectric correlations from ferroelectric and noncollinear magnetic modifications, and notably these reflections are absent at the Mn K edge.

The principal features of data displayed in Fig. 2 are near symmetry about our origin at 90°, with maxima at $\psi=0°$, π, and zero at $\psi=\pi/2$ with respect to this origin. Looking to assign the diffraction event to the E1-E1 process, suggested by Mannix *et al.*,[20] we find from Eq. (C2) that principal features are in accord with an amplitude that is a coherent sum of multipoles of the form $(t-\cos\psi+d\cos 2\psi)$ together with an overall scale factor. The parameters t and d are to be determined, and the parameter with $\cos\psi$ is chosen to make the intensity at $\psi=\pi$ exceed the intensity at $\psi=0°$. Requiring the amplitude to be zero at $\psi=\pi/2$ leads to $t=d$. However, zeroes in the data are actually separated by 200°, to a good approximation, and the departure from 180° is taken to be a real effect that must be accounted for by a successful analysis. In a move toward this goal, we have fitted data to $(t-\cos\psi+d\cos 2\psi+u\sin\psi+w\sin 2\psi)^2$, where additional coherent sine terms are again suggested by the E1-E1 structure factor in the π'-σ channel of diffraction [Eq. (C2)]. The satisfactory agreement between data and this expression for the intensity shown in Fig. 2 is achieved with parameters

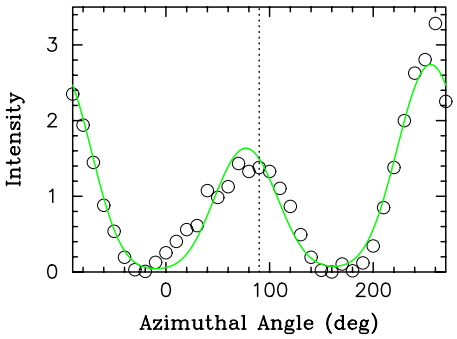

FIG. 2. (Color online) Data collected in the π'-σ channel at C-type reflections in phase (ii) are reproduced from Fig. 20 in Mannix *et al.* (Ref. 20). The data were taken with a primary energy corresponding to the E1-E1 event around 7.520 keV in the vicinity of the Tb L_3 edge. The solid curve is a fit to intensity proportional to $\{t-\cos\psi+d\cos 2\psi+u\sin\psi+w\sin 2\psi\}^2$, where the origin of the azimuthal angle, ψ, is denoted by a vertical line, displaced by 90° from the origin used by Mannix *et al.*, and the fit yields $t=4.97$, $d=3.20$, $u=0.48$, and $w=-1.67$. The physical content of the parameters is the subject of Sec. III C.

given in the figure caption. Most notably, t and d are significantly different from one another.

Turning next to data gathered in the σ'-σ channel, no intensity is found for $\psi=-70°$ at the energy identified with the E1-E1 process. Null intensity in the σ'-σ channel of the E1-E1 process for all ψ is achieved by equating to zero all four parity-even multipoles of the form $A^t_{K,Q}$ with $K=0$ and 2, as can be seen by reference to Eq. (C1). Inspection of Eq. (C2) shows that this step sets parameters d and w in the E1-E1 structure factor in the π'-σ channel equal to zero, i.e., it is not possible for the E1-E1 process to both generate $\cos 2\psi$ and $\sin 2\psi$ in the π'-σ channel of diffraction and, also, null diffraction in the σ'-σ channel of diffraction. Thus we seek an alternative physical origin for the existence of parameters d and w in the π'-σ channel.

To this end note that intensity at C-type reflections is observed in the σ'-σ channel but at an energy of about 7 eV below the maximum of intensity in the π'-σ channel, which is attributed to the E1-E1 process. As a function of the azimuthal angle, intensity in the σ'-σ channel follows $\sin^2\psi$.

Let us explore the possibility that intensity in the σ'-σ channel is due to an E2-E2 process and that this process also contributes in the π'-σ channel the parameters we label as d and w, and with them contributions which are proportional to $\cos 2\psi$ and $\sin 2\psi$, respectively.

Inspection of Eq. (E1) for the σ'-σ amplitude in the E2-E2 process shows the existence of a suitable contribution, proportional to $A^t_{1,1}\sin\psi$. A contribution $A^t_{1,1}\cos\psi$ appears also in the π'-σ amplitude (E2), where $\sin 2\psi$ is generated by $A^t_{2,0}$ $A^t_{2,2}$, and $B^t_{3,2}$ while $\cos 2\psi$ is generated by $A^t_{2,1}$. However, all multipoles $A^t_{K,Q}$ with $K=2$ arise in the σ'-σ channel of the E1-E1 process where they are set to zero, in order to fit the corresponding experimental data, and the same must be true in the E2-E2 process by reason of their common rotational symmetry (multipoles in E1-E1 and E2-E2 processes share parity, time reversal, and angular symmetry.[6]) Thus the essential contribution to the π'-σ amplitude, $d\cos 2\psi$, cannot arise from the E2-E2 process. As we shall now see, all features suggested by the experimental data for both the σ'-σ channel and the π'-σ channel can be met by contributions from the magnetoelectric (time-odd and parity-odd) amplitude that add coherently to specified contributions from the E1-E1 amplitude.

TABLE I. Contributions to diffraction at C-type reflections. Entries for $(\pi'$-$\sigma)$ and $(\sigma'$-$\sigma)$ are inferred by data (Ref. 20). The implication for $(\pi'$-$\pi)$ is also included.

	Const.	$\cos(\psi)$	$\cos(2\psi)$	$\sin(\psi)$	$\sin(2\psi)$
			$(\pi'$-$\sigma)$		
E1-E1	$B^t_{1,1}$	$A^t_{1,1}$, $B^t_{2,1}$		$A^t_{1,0}$, $B^t_{2,2}$	
E1-E2		$A^g_{1,0}$, $B^g_{2,2}$	$B^g_{3,2}$		$A^g_{2,1}$, $B^g_{3,1}$, $B^g_{3,3}$
			$(\sigma'$-$\sigma)$		
E1-E2				$A^g_{1,0}$, $B^g_{2,2}$	
			$(\pi'$-$\pi)$		
E1-E1		$A^t_{1,0}$		$A^t_{1,1}$	
E1-E2				$A^g_{1,0}$, $B^g_{2,2}$	

First, a contribution proportional to $\sin\psi$ is present in the magnetoelectric σ'-σ amplitude (D4) and no such contribution is found in the polar σ'-σ amplitude (D1). Looking in detail at Eq. (D4) for the magnetoelectric σ'-σ amplitude, we see that observed intensity in the σ'-σ channel, found at an energy 7 eV below the main E1-E1 diffraction, can be attributed to multipoles $A^g_{1,0}$ and $B^g_{2,2}$ with $A^g_{1,0}$ proportional to the Tb anapole.[6] We recall that the g (u) superscript labels parity-odd and time-odd (time-even) multipoles. The contribution from these two multipoles in the π'-σ amplitude (D5) is proportional to $\cos\psi$. Second, in the π'-σ amplitude (D5), contributions proportional to $\cos 2\psi$ and $\sin 2\psi$ are accompanied by multipoles $B^g_{3,2}$, and $A^g_{2,1}$, $B^g_{3,1}$, and $B^g_{3,3}$, respectively, none of which contribute in the σ'-σ amplitude (D4). In consequence, the magnetoelectric amplitude can be held solely responsible for observed intensity in the σ'-σ channel while, simultaneously, completing a successful account of intensity observed in the π'-σ channel by providing a physical origin of parameters we label as d and w. Our findings for C-type reflections are gathered in Table I together with the implication for the π'-π channel.

The foregoing scenario for C-type reflections is consistent with Tb magnetization parallel to b and c, as in Secs. III A and III B. For the parameter t is proportional to $B^t_{1,1}$ which may be magnetization along b, and the parameter u contains $A^t_{1,0}$ which may be magnetization along c. Here we appeal to Eq. (B5) with $K=1$.

The collection of multipoles in Table I is not consistent with structure factors (A2) and (A3) for Tb ions in the room-temperature structure, *Pbnm*. Even so it might be relevant in the analysis of C-type reflections that $\tan(\epsilon)=22.72$ with $k=3$, which implies that diffraction in the E1-E1 channel is strongly suppressed, thus making E1-E1 and E1-E2 amplitudes comparable.

A completely plausible model for electron structure that successfully simulates C-type reflections is obtained from

the following considerations. The multipoles gathered in Table I are compatible with a structure factor of the form $\langle T_Q^K\rangle - (-1)^Q \langle T_{-Q}^K\rangle$ for parity-even multipoles and a similar result for parity-odd multipoles. Using Eq. (B5) for *C*-type reflections and the suggested structure factors, one finds that all $A_{K,Q}^t$ and $A_{K,Q}^g$ are zero. The corresponding σ'-σ component of the E1-E1 amplitude is zero, as required. With just one constraint, namely, $B_{2,1}^g=0$, the σ'-σ component of the E1-E2 amplitude is proportional to $\sin(\psi)$, as required [from Table I, the π'-π component of the E1-E1 amplitude is predicted to be zero while the π'-π component of the E1-E2 amplitude is predicted to be proportional to $B_{2,2}^g \sin(\psi)$].

The foregoing constraint, on a particular component of the magnetoelectric quadrupole, can be implemented in a handed (chiral) cycloidal model of electron structure that simultaneously allows other $B_{K,Q}^g$ to be different from zero. For there to be agreement with data reproduced in Fig. 2, one finds that projections of a Tb dipole moment on the *b* and *c* axes must be different from zero. While the structure factor in Appendix F for a chiral cycloidal structure traced out in the *b*-*c* plane, with a pitch=1/25 and fractional wave vector=7/25, offers a detailed simulation of *C*-type reflections, there are insufficient experimental data to fully define the model in terms of magnetoelectric moments $\langle G_Q^K\rangle$, at this point in time.

Our study shows that a neutral achiral cycloidal model, with a pitch=1/4, is incompatible with the experimental data reproduced here in Fig. 2. This finding is at odds with the analysis reported by Mannix *et al.* in Ref. 20.

D. Phase (iii)

Below 7 K and the primary energy tuned to the Tb L_3 edge, diffraction appears in the π'-σ channel at the reflection (0, 4–0.42, 0), whereas ordering with $\mathbf{q}=0.28\mathbf{b}^*$ occurs on the Mn sublattice. No diffraction at (0, 4–0.42, 0) is visible at the Mn *K* edge.

As a function of azimuthal-angle intensity follows a $\cos^2\psi$ dependence. This dependence of the intensity in the π'-σ channel can arise from multipoles in $A_{1,1}^t$ and $B_{2,1}^t$ which arise in the E1-E1 event (C2). We note that, the quadrupole order is forbidden in the room-temperature structure *Pbmn*, where the projection *Q* is restricted to even integers and, also, neither $A_{1,1}^t$ or $B_{2,1}^t$ generate diffraction in the σ'-σ channel, in accord with observations. Thus intensity at (0, 4–0.42, 0) that sets in below 7 K, and is exclusive to Tb ions, can arise from the onset of long-range magnetic order with a motif that allows $A_{1,1}^t$ to be different from zero, or an additional distortion of the lattice, described by $B_{2,1}^t$. If there is correspondence between angular components of Ψ_Q^K and angular components of electronic structure, as implied by previous findings in this section, $A_{1,1}^t$ is proportional to Tb magnetization along the *a* axis, for which we find no evidence in phases (i) and (ii). Moreover, quadrupoles in $B_{2,1}^t$ will have angular symmetry *yz*. In arriving at these relations we use Eq. (B5) with $K=1$ and 2.

IV. CONCLUSIONS

We present a careful analysis in terms of atomic multipoles of the azimuthal-scan dependence of selected reflections (presented in Ref. 20) in $TbMnO_3$. The azimuthal-scan dependence of *C*-type reflection has allowed establishment of the resonant events, E1-E1 and E1-E2, which are the source of the diffracted intensities. Contributions from E2-E2 events are negligible. A chiral cycloidal structure for the Tb ions traced out in the *b*-*c* plane is compatible with the observed azimuthal-scan dependence. Unfortunately it is not possible to further model the data in terms of the magnetoelectric moments due to lack of experimental data. However, our results represent a step forward in establishing the nature of the changes in the electronic and magnetic structures as the sample undergoes the collinear to cycloidal and ferroelectric phase transitions. We hope this work will stimulate further experiments on $TbMnO_3$ which would make possible precisely identifying of the role of the active multipoles in the different phases. Particularly interesting is the fact that our conclusions do not rely on the knowledge of the low-temperature structure of the material, which is still uncertain.

ACKNOWLEDGMENTS

One of us (S.W.L.) is grateful to A. T. Boothroyd, P. J. Brown, L. C. Chapon, K. S. Knight, and L. Paolasini for various helpful discussions and comments. The analysis of data and preparation of Fig. 2 were performed by Devinda Sivia. We thank D. F. McMorrow for inspiring our interest in resonant x-ray diffraction by terbium manganate and permission to reproduce data from Mannix *et al.* (Ref. 20).

APPENDIX A: ATOMIC MULTIPOLES AND UNIT-CELL STRUCTURE FACTORS

Ground-state electron structure at the site of a resonant ion is described by atomic multipoles of rank *K*, with $K=0$ (scalar and angularly isotropic), $K=1$ (dipole), $K=2$ (quadrupole), $K=3$ (octupole), etc. A multipole is the mean value, or expectation value, of an operator equivalent. In many crystals any Templeton-Templeton scattering is due to a parity-even quadrupole, which can be represented by $\langle J_\alpha J_\beta\rangle$, where J_α is an angular-momentum operator, in which α labels a spatial component, and angular brackets denote the expectation value. Because J_α is time odd and parity even, the quadrupole operator equivalent, $J_\alpha J_\beta$, is both time even and parity even. With long-range magnetic order in a crystal, which breaks time-reversal symmetry, $\langle J_\alpha\rangle \neq 0$. Then it might be appropriate to use the identity $\langle J_\alpha J_\beta\rangle = \langle J_\alpha\rangle\langle J_\beta\rangle + \langle \Delta J_\alpha \Delta J_\beta\rangle$, where $\Delta J_\alpha = J_\alpha - \langle J_\alpha\rangle$, and the fluctuation $\langle \Delta J_\alpha \Delta J_\beta\rangle$ contributes Templeton-Templeton scattering. A multipole can be different from zero only if it obeys all symmetry operations in the point group for the environment of the resonant ion, which is a statement of Neumann's principle.

Bragg diffraction measures a coherent sum of multipoles in a unit-cell accompanied by the usual spatial phase factors, and the sum of multipoles of rank *K* is denoted by Ψ^K. The configuration of multipoles in Ψ^K is proscribed by symmetry in the crystal space group. In parity-even channels of diffraction, E1-E1 and E2-E2, say, space-group allowed reflections satisfy $\Psi^0 \neq 0$, a condition tantamount to extinction rules for

the reflection. In general, angular components of Ψ^K do not map directly on to angular components of the electron structure. The presence of multiaxis noncollinear order in the crystal is one case where it is unsafe to assume correspondence between angular components of Ψ^K and electron structure.

A calculation of Ψ_Q^K for ions using positions 4b in *Pbnm* is described in Sec. 6.3 of Ref. 6. It is found that there is a selection rule on Q imposed by the space group, namely, diffraction is allowed for even $l+Q$ while none is generated by the point group. For Mn ions in terbium manganate we find

$$\Psi_Q^{t,K}(\mathrm{Mn}) = (1+(-1)^{l+Q})[\langle T_Q^K\rangle + (-1)^{h+k}(-1)^K\langle T_{-Q}^K\rangle], \tag{A1}$$

where superscript t is added in $\Psi_Q^{t,K}$ to denote the fact that it is a sum of parity-even multipoles $\langle T_Q^K\rangle$. These multipoles arise in E1-E1 and E2-E2 events (Appendixes C and E) and possess the property of one-to-one correspondence between rank, K, and symmetry with respect to time reversal; even (odd) K is time even (odd).[6] Applied to terbium manganate at room temperature, in Eq. (A1) we should set K equal to an even integer. Operator equivalents for T_Q^1 and T_Q^2, for example, are angular momentum J_Q and a tensor product $\{J\otimes J\}_Q^2$, respectively.

Terbium ions in terbium manganate have fractional atomic positions $x=-0.0149(8)$, $y=0.0798(7)$, and $z=\frac{1}{4}$.[10] We find

$$\Psi_Q^{t,K}(\mathrm{Tb}) = 2[\cos(\epsilon)\langle T_Q^K\rangle + \cos(\epsilon')(-1)^{K+Q}(-1)^{h+k+l}\langle T_{-Q}^K\rangle], \tag{A2}$$

$$\Psi_Q^{u,K}(\mathrm{Tb}) = 2i[\sin(\epsilon)\langle U_Q^K\rangle + -\sin(\epsilon')(-1)^{K+Q}(-1)^{h+k+l} \times\langle U_{-Q}^K\rangle], \tag{A3}$$

where $\epsilon=2\pi\ (xh+yk+zl)$ and $\epsilon'=\epsilon-4\pi yk$. In Eq. (A3) the superscript, u, in $\Psi_Q^{u,K}$ denotes polar multipoles $\langle U_Q^K\rangle$, with $K=1$, 2, or 3 for E1-E2, which are parity odd and time even, i.e., they can be different from zero in the absence of long-range magnetic order. Operator equivalent for U_Q^1 and U_Q^2 are n_Q and $\{\boldsymbol{L}\otimes\boldsymbol{\Omega}\}_Q^2$, respectively, where n_Q is a unit (polar) vector, and $\boldsymbol{L}$ and $\boldsymbol{\Omega}$ are operators for orbital angular momentum and an anapole.[6,12] (In Ref. 6 it is shown that the E1-E2 amplitude reported in Ref. 12 is not correct.) Invariance to the point group, represented by inversion $\otimes C_{2z}$, means $\langle T_Q^K\rangle$ must have even Q and $\langle U_Q^K\rangle$ must have odd Q. In consequence, complex conjugates satisfy $\langle T_Q^K\rangle^*=\langle T_{-Q}^K\rangle$ and $\langle U_Q^K\rangle^*=-\langle U_{-Q}^K\rangle$. Our phase convention for real and imaginary parts of any quantity, Z, say, is $Z=Z'+iZ''$.

Space-group allowed reflections from the room-temperature structure are those for which Eqs. (A1) and (A2) with $Q=0$ and even K can be different from zero. Diffraction from Mn ions is allowed for even $h+k$ and even l, and diffraction at $(h,0,l)$ from Tb ions is allowed for even $h+l$. For space-group forbidden reflections from Mn ions, $l+Q$ is even and $h+k$ is odd. In particular, reflections $(0,k,0)$ with odd k have even Q, and $B_{K,2}^t=-\Psi_{+2}^{t,K}=-4i\langle T_{+2}^K\rangle''$ and all other components in Eq. (B5) are zero. The same results apply at $(h,0,0)$ with odd h except for a sign change, namely, $B_{K,2}^t=\Psi_{+2}^{t,K}=4i\langle T_{+2}^K\rangle''$. At the terbium E1 energy for reflections $(h,0,0)$ with odd h, the room-temperature structure (A2) yields even Q, and $\Psi_Q^{t,K}=-\Psi_{-Q}^{t,K}$. Hence, at reflections $(h,0,0)$ with odd h, $B_{K,2}^t=\Psi_{+2}^{t,K}=4i\cos(2\pi xh)\langle T_{+2}^K\rangle''$ and $A_{K,0}^t=A_{K,2}^t=0$.

APPENDIX B: AZIMUTHAL-ANGLE SCAN

Given knowledge of the space group, one can construct unit-cell structure factors and several examples are listed in Ref. 6. In the absence of this knowledge it pays dividends to write Ψ_Q^K, written in the coordinate space (x,y,z), as a sum of quantities that are even (A_Q^K) and odd (B_Q^K) functions of the projection Q with $-K\le Q\le K$. In this case, the rotation matrix $\boldsymbol{D}^K\equiv\boldsymbol{D}^K(\psi)$ in Eq. (1) fulfills one task: that of rotation of the crystal about the x axis through an angle ψ. In place of Eq. (1) we write,

$$F_{\mu\nu} = \sum_K \boldsymbol{J}_{\mu\nu}^K\cdot\boldsymbol{D}^K(\psi)\cdot(\boldsymbol{A}^K+\boldsymbol{B}^K). \tag{B1}$$

In Eq. (B1),

$$A_Q^K + B_Q^K = \sum_q \boldsymbol{D}_{Qq}^K(\Omega)\Psi_q^K, \tag{B2}$$

where $\boldsymbol{D}_{Qq}^K(\Omega)$ is an element of a rotation matrix, also called the Wigner D function,[23] in which Ω denotes the three Euler angles used to specify the setting of the crystal at $\psi=0°$ in coordinates (x,y,z).[6,23] By definition, the change $Q\to-Q$ in Eq. (B2) leads to

$$A_Q^K - B_Q^K = \sum_q \boldsymbol{D}_{-Qq}^K(\Omega)\Psi_q^K. \tag{B3}$$

Euler angles Ω depend on the direction of the Bragg wave vector relative to axes in the crystal. In some cases (hexagonal and monoclinic cells, for example), it is necessary to erect right-handed orthonormal axes of quantization (ξ,η,ζ), say, for a reference ion in the unit cell that do not coincide with cell edges. The direction of the Bragg wave vector is specified in coordinates (ξ,η,ζ) that nominally coincide with (x,y,z). For example, if the Bragg wave vector is parallel to the z axis, Ω specifies a clockwise (left-handed) rotation of the crystal by 90° about the y axis, aligning the Bragg wave vector with $-\mathbf{x}$. If the Bragg wave vector is confined to the plane of scattering, the alignment is achieved by a simple rotation of the crystal about the z axis.

In the latter case, $A_Q^K+B_Q^K=e^{iQ\alpha}\Psi_Q^K$, where α is the angle of rotation about the z axis,[6] and

$$A_Q^K = \frac{1}{2}(e^{iQ\alpha}\Psi_Q^K + e^{-iQ\alpha}\Psi_{-Q}^K) = A_{-Q}^K,$$

$$B_Q^K = \frac{1}{2}(e^{iQ\alpha}\Psi_Q^K - e^{-iQ\alpha}\Psi_{-Q}^K) = -B_{-Q}^K. \tag{B4}$$

Should the crystal possess orthonormal cell edges a, b, and c, which nominally coincide with axes in coordinates (x,y,z), settings of the crystal for reflections $(h,0,0)$ and $(0,k,0)$ are

achieved with $\alpha=\pi$ and $\pi/2$, respectively. Considering $(0,k,0)$ and $Q=0$, 1, and 2, we find from Eq. (B4),

$$A_0^K = \Psi_0^K,$$

$$A_1^K = \frac{i}{2}(\Psi_{+1}^K - \Psi_{-1}^K), \quad A_2^K = -\frac{1}{2}(\Psi_{+2}^K + \Psi_{-2}^K),$$

$$B_1^K = \frac{i}{2}(\Psi_{+1}^K + \Psi_{-1}^K), \quad B_2^K = -\frac{1}{2}(\Psi_{+2}^K - \Psi_{-2}^K). \tag{B5}$$

Returning to correspondence between angular components of Ψ_Q^K, and angular components of electronic structure that are defined with respect to crystal axes (a,b,c)—more generally the axes of quantization (ξ,η,ζ)—A_1^1 need not be parallel to the a axis and B_1^1 need not be parallel to the b axis. Examples of electron structures with angular components that do not directly map to components of Ψ_Q^K are found in Appendix F, which deals with noncollinear cycloidal structures. [Spherical, R_q with $q=0$ and ± 1, and Cartesian, R_α with $\alpha=x,y,z$, components of a vector $(K=1)$ are related by $R_x=\frac{1}{\sqrt{2}}(R_{-1}-R_{+1})$, $R_y=\frac{i}{\sqrt{2}}(R_{-1}+R_{+1})$, and $R_z=R_0$].

An element of the rotation matrix in Eq. (B1) is[6]

$$D_{QQ'}^K(\psi) = e^{iQ(\pi/2)} d_{QQ'}^K(\psi) e^{-iQ'(\pi/2)}, \tag{B6}$$

where $d_{QQ'}^K(\psi)$ is a real function whose properties are reviewed in Ref. 23, for example. The property $d_{QQ'}^K(0) = \delta_{QQ'}$ means that for $\psi=0°$ the crystal is at the setting in coordinates (x,y,z) fixed by Euler angles Ω. The sense of rotation is counter clockwise when viewed down the Bragg wave vector.

APPENDIX C: E1-E1; UNIT-CELL STRUCTURE FACTORS

$$F_{\sigma'\text{-}\sigma}^{t(\mathrm{E1-E1})} = -\frac{1}{\sqrt{3}}A_{0,0}^t + \frac{\sqrt{6}}{4}\left[\cos(2\psi) + \frac{1}{3}\right]A_{2,0}^t - i\,\sin(2\psi)A_{2,1}^t + \frac{1}{2}[\cos(2\psi) - 1]A_{2,2}^t, \tag{C1}$$

$$F_{\pi'\text{-}\sigma}^{t(\mathrm{E1-E1})} = -\frac{1}{\sqrt{2}}i\,\cos(\theta)\sin(\psi)A_{1,0}^t + \cos(\theta)\cos(\psi)A_{1,1}^t + i\,\sin(\theta)B_{1,1}^t - \frac{\sqrt{6}}{4}\sin(\theta)\sin(2\psi)A_{2,0}^t + -i\,\sin(\theta)\cos(2\psi)A_{2,1}^t$$
$$-\cos(\theta)\cos(\psi)B_{2,1}^t - \frac{1}{2}\sin(\theta)\sin(2\psi)A_{2,2}^t + i\,\cos(\theta)\sin(\psi)B_{2,2}^t, \tag{C2}$$

$$F_{\pi'\text{-}\pi}^{t(\mathrm{E1-E1})} = -\frac{1}{\sqrt{3}}\cos(2\theta)A_{0,0}^t + \frac{i}{\sqrt{2}}\sin(2\theta)\cos(\psi)A_{1,0}^t + \sin(2\theta)\sin(\psi)A_{1,1}^t + \frac{1}{\sqrt{6}}\{\sin^2(\theta)[3\,\cos^2(\psi) - 1] - 1\}A_{2,0}^t$$
$$-i\,\sin^2(\theta)\sin(2\psi)A_{2,1}^t + [1 - \sin^2(\theta)\sin^2(\psi)]A_{2,2}^t. \tag{C3}$$

In Eq. (B1) $J_Q^K=(-1)^Q X_{-Q}^K$, where X_{-Q}^K is found in Table III of Ref. 6.

We note the following properties of the E1-E1 unit-cell structure factors. (a) $F_{\sigma'\text{-}\sigma}^t$ and $F_{\pi'\text{-}\pi}^t$ are functions of $A_{K,Q}^t$ only; (b) $F_{\sigma'\text{-}\sigma}^t$ is independent of the Bragg angle, θ, and a function of 2ψ; (c) $F_{\pi'\text{-}\pi}^t$ is a function 2θ, and it contains harmonics of ψ and 2ψ in addition to a constant proportional to $A_{0,0}^t$ which may vanish at a space-group forbidden reflection; (d) $F_{\pi'\text{-}\sigma}^t$ contains harmonics of ψ and 2ψ and no constant, and contributions depend on either sin θ or cos θ; and (e) $F_{\pi'\text{-}\sigma}^t$ and $F_{\sigma'\text{-}\pi}^t$ are related by sign change to all $A_{K,Q}^t$.

APPENDIX D: E1-E2; UNIT-CELL STRUCTURE FACTORS

1. Polar

$$F_{\sigma'\text{-}\sigma}^u = -\frac{i\sqrt{6}}{5}\sin(\theta)B_{1,1}^u - \frac{i\,\sin(\theta)}{\sqrt{20}}\sin(2\psi)A_{2,0}^u + \frac{2\,\sin(\theta)}{\sqrt{30}}\cos(2\psi)A_{2,1}^u - \frac{i\,\sin(\theta)}{\sqrt{30}}\sin(2\psi)A_{2,2}^u - \frac{i\,\sin(\theta)}{5\sqrt{6}}[5\,\cos(2\psi) + 3]B_{3,1}^u$$
$$-\frac{2\,\sin(\theta)}{\sqrt{15}}\sin(2\psi)B_{3,2}^u + \frac{2i\,\sin(\theta)}{\sqrt{10}}\sin^2(\psi)B_{3,3}^u, \tag{D1}$$

$$F^u_{\pi'\text{-}\sigma} = \frac{i\sqrt{3}}{10}\sin(2\theta)\cos(\psi)A^u_{1,0} + \frac{3}{5\sqrt{6}}\sin(2\theta)\sin(\psi)A^u_{1,1} + \frac{i}{4\sqrt{5}}\{\cos(2\theta)[5\cos^2(\psi) - 3] - \sin^2(\psi)\}A^u_{2,0} + \frac{1}{2\sqrt{30}}[5\cos(2\theta) + 1]\sin(2\psi)A^u_{2,1} + \frac{2i}{\sqrt{30}}\sin(2\theta)\sin(\psi)B^u_{2,1} + \frac{i}{2\sqrt{30}}\{2\sin^2(\theta) + [5\cos(2\theta) + 1]\cos^2(\psi)\}A^u_{2,2} - \frac{2}{\sqrt{30}}\sin(2\theta)\cos(\psi)B^u_{2,2} - \frac{i}{5\sqrt{2}}\sin(2\theta)\cos(\psi)A^u_{3,0} - \frac{1}{5\sqrt{6}}\sin(2\theta)\sin(\psi)A^u_{3,1} + \frac{i}{\sqrt{6}}\sin^2(\theta)\sin(2\psi)B^u_{3,1} + \frac{i}{\sqrt{15}}\sin(2\theta)\cos(\psi)A^u_{3,2} - \frac{2}{\sqrt{15}}\cos(2\psi)\sin^2(\theta)B^u_{3,2} + \frac{\sin(2\theta)}{\sqrt{10}}\sin(\psi)A^u_{3,3} + \frac{i\sin^2(\theta)}{\sqrt{10}}\sin(2\psi)B^u_{3,3}, \tag{D2}$$

$$F^u_{\pi'\text{-}\pi} = -\frac{i\sqrt{6}}{5}\sin(3\theta)B^u_{1,1} + \frac{i}{2\sqrt{5}}\sin(3\theta)\sin(2\psi)A^u_{2,0} - \frac{2}{\sqrt{30}}\sin(3\theta)\cos(2\psi)A^u_{2,1} + \frac{i}{\sqrt{30}}\sin(3\theta)\sin(2\psi)A^u_{2,2} + \frac{2i}{5\sqrt{6}}\sin^3(\theta)[3\sin^2(\psi) - \cos(2\psi) + 3\cot^2(\theta)]B^u_{3,1} - \frac{2}{\sqrt{15}}\sin^3(\theta)\sin(2\psi)B^u_{3,2} - \frac{2i}{\sqrt{10}}\sin(\theta)[\cos^2(\psi) + \cos^2(\theta)\sin^2(\psi)]B^u_{3,3}. \tag{D3}$$

An application of Eq. (B1) to polar multipoles has $J^K_Q = i^{K-1}(-1)^Q(\tilde{N}^K_{-Q} - N^K_{-Q})$ in which x-ray spherical tensors are found in Table V in Ref. 6. The following properties of the unit-cell structure factors merit note: (a) $F^u_{\sigma'\text{-}\sigma}$ and $F^u_{\pi'\text{-}\pi}$ have contributions that do not depend on ψ; (b) in the unrotated channels, $F^u_{\sigma'\text{-}\sigma}$ and $F^u_{\pi'\text{-}\pi}$, even-rank contributions are composed of $A^u_{K,Q}$ and the odd-rank contribution is composed of $B^u_{K,Q}$ (it is appropriate to recall that, in parity-odd events, odd-rank multipoles are true spherical tensors while even-rank multipoles are pseudotensors, e.g., the E1-M1 event contains a multipole of rank zero which is related to the chirality of the material, a material property with transformation credentials that match the helicity of a beam of x rays.); (c) $F^u_{\pi'\text{-}\sigma}$ and $F^u_{\sigma'\text{-}\pi}$ are related by a simultaneous overall change of sign to the unit-cell structure factors and the substitution $\theta \rightarrow -\theta$.

2. Magnetoelectric

$$F^g_{\sigma'\text{-}\sigma} = -\frac{\sqrt{3}}{5}\cos(\theta)\sin(\psi)A^g_{1,0} - \frac{i\sqrt{6}}{5}\cos(\theta)\cos(\psi)A^g_{1,1} + \frac{2\cos(\theta)}{\sqrt{30}}\cos(\psi)B^g_{2,1} - \frac{2i}{\sqrt{30}}\cos(\theta)\sin(\psi)B^g_{2,2} + \frac{\sqrt{2}}{5}\cos(\theta)[1 - 5\cos^2(\psi)]\sin(\psi)A^g_{3,0} + \frac{2i}{\sqrt{6}}\cos(\theta)\cos(\psi)[11 - 15\cos^2(\psi)]A^g_{3,1} + \frac{2}{\sqrt{15}}\cos(\theta)[1 - 3\cos^2(\psi)]\sin(\psi)A^g_{3,2} + \frac{i\cos(\theta)}{\sqrt{10}}\sin(\psi)\sin(2\psi)A^g_{3,3}, \tag{D4}$$

$$F^g_{\pi'\text{-}\sigma} = \frac{\sqrt{3}}{10}\sin(2\theta)\cos(\psi)A^g_{1,0} - \frac{3i}{5\sqrt{6}}\sin(2\theta)\sin(\psi)A^g_{1,1} + \frac{1}{4\sqrt{5}}\{\cos(2\theta)[1 + \cos^2(\psi)] - \sin^2(\psi)\}A^g_{2,0} - \frac{i\cos^2(\theta)}{\sqrt{30}}\sin(2\psi)A^g_{2,1} - \frac{2}{\sqrt{30}}\sin(2\theta)\sin(\psi)B^g_{2,1} + \frac{1}{\sqrt{30}}\{\cos^2(\theta)[1 + \cos^2(\psi)] - 3\cos(2\theta)\}A^g_{2,2} - \frac{2i\sin(2\theta)}{\sqrt{30}}\cos(\psi)B^g_{2,2} - \frac{\sin(2\theta)}{5\sqrt{2}}\cos(\psi) \times [5\cos^2(\psi) - 4]A^g_{3,0} + \frac{i\sin(2\theta)}{5\sqrt{6}}\sin(\psi)[15\cos^2(\psi) - 4]A^g_{3,1} + \frac{\cos^2(\theta)}{\sqrt{6}}\sin(2\psi)B^g_{3,1} - \frac{\sin(2\theta)}{\sqrt{15}}\cos(\psi)[3\cos^2(\psi) - 2]A^g_{3,2} + \frac{2i}{\sqrt{15}}\cos^2(\theta)\cos(2\psi)B^g_{3,2} + \frac{i}{2\sqrt{10}}\sin(2\theta)\sin(2\psi)\cos(\psi)A^g_{3,3} + \frac{\cos^2(\theta)}{\sqrt{10}}\sin(2\psi)B^g_{3,3}, \tag{D5}$$

$$F^g_{\pi'\text{-}\pi} = -\frac{\sqrt{3}}{5}\cos(3\theta)\sin(\psi)A^g_{1,0} - \frac{i\sqrt{6}}{5}\cos(3\theta)\cos(\psi)A^g_{1,1} - \frac{2\cos(3\theta)}{\sqrt{30}}\cos(\psi)B^g_{2,1} + \frac{2i}{\sqrt{30}}\cos(3\theta)\sin(\psi)B^g_{2,2} + \frac{\sqrt{2}}{5}\cos(\theta)\sin(\psi)[2 - 5\cos^2(\psi)\sin^2(\theta) - \cos^2(\theta)]A^g_{3,0} + \frac{2i}{5\sqrt{6}}\cos(\theta)\cos(\psi)\{\cos^2(\theta) + \sin^2(\theta)[12 - 15\cos^2(\psi)]\}A^g_{3,1} - \frac{2\cos(\theta)}{\sqrt{15}}\sin(\psi)[\cos^2(\theta) + 3\cos^2(\psi)\sin^2(\theta)]A^g_{3,2} - \frac{i}{2\sqrt{10}}\cos(\psi)\{\cos(\theta)[3 + \cos^2(\psi)] + \cos(3\theta)\sin^2(\psi)\}A^g_{3,3}. \tag{D6}$$

Equation (B1) applied to magnetoelectric multipoles has $J_Q^K=-i^K(-1)^Q(\tilde{N}_{-Q}^K+N_{-Q}^K)$ in which x-ray spherical tensors are found in Table V in Ref. 6. The following properties of unit-cell structure factors merit note: (a) in the unrotated channels, $F_{\sigma'\text{-}\sigma}^g$ and $F_{\pi'\text{-}\pi}^g$, the odd-rank contribution is composed of $A_{K,Q}^g$ and the even-rank contributions are composed of $B_{K,Q}^g$, which is an opposite order to contributions to polar structure factors considered above; (b) unit-cell structure factors for rotated channels $F_{\pi'\text{-}\sigma}^g$ and $F_{\sigma'\text{-}\pi}^g$ are related by the simple substitution $\theta\rightarrow-\theta$; (c) in the four channels of polarization all contributions depend on the azimuthal angle and there are no constant terms.

APPENDIX E: E2-E2; UNIT-CELL STRUCTURE FACTORS

$$
\begin{aligned}
F_{\sigma'\text{-}\sigma}^{t(\mathrm{E2\text{-}E2})} = {} & \frac{1}{2\sqrt{5}}\cos(2\theta)A_{0,0}^t - \frac{i}{2\sqrt{10}}\sin(2\theta)\cos(\psi)A_{1,0}^t - \frac{1}{\sqrt{20}}\sin(2\theta)\sin(\psi)A_{1,1}^t + \frac{1}{4\sqrt{14}}[\cos(2\theta) - 3\cos(2\theta)\cos^2(\psi) \\
& - 3\sin^2(\psi)]A_{2,0}^t - \frac{3i}{2\sqrt{21}}\sin^2(\theta)\sin(2\psi)A_{2,1}^t + \frac{3}{4\sqrt{21}}[1 + \cos(2\theta)\sin^2(\psi) + \cos^2(\psi)]A_{2,2}^t + \frac{i}{2\sqrt{10}}\sin(2\theta)[5\cos^2(\psi) \\
& - 3]\cos(\psi)A_{3,0}^t + \frac{3}{2\sqrt{30}}[5\cos^2(\psi) - 1]\sin(2\theta)\sin(\psi)A_{3,1}^t - \frac{3i}{2\sqrt{3}}\sin(2\theta)\sin^2(\psi)\cos(\psi)A_{3,2}^t - \frac{\sin(2\theta)}{2\sqrt{2}}\sin^3(\psi)A_{3,3}^t \\
& - \frac{1}{2\sqrt{70}}\{[35\cos^4(\psi) - 30\cos^2(\psi) + 3]\cos^2(\theta) - 5\cos^2(\psi) + 1\}A_{4,0}^t + \frac{i}{2\sqrt{14}}\{[14\cos^2(\psi) - 6]\cos^2(\theta) \\
& - 1\}\sin(2\psi)A_{4,1}^t + \frac{1}{\sqrt{7}}[8\cos^2(\theta)\cos^2(\psi) - \cos^2(\psi) - \cos^2(\theta) - 7\cos^4(\psi)\cos^2(\theta)]A_{4,2}^t + \frac{i}{2\sqrt{2}}\sin(2\psi)[1 \\
& - 2\cos^2(\theta)\sin^2(\psi)]A_{4,3}^t + \frac{1}{4}[1 - \cos(2\theta)\sin^2(\psi) + \cos^2(\psi)]\sin^2(\psi)A_{4,4}^t, \qquad \text{(E1)}
\end{aligned}
$$

$$
\begin{aligned}
F_{\pi'\text{-}\sigma}^{t(\mathrm{E2\text{-}E2})} = {} & + \frac{i\cos(3\theta)}{2\sqrt{10}}\sin(\psi)A_{1,0}^t - \frac{\cos(3\theta)}{2\sqrt{5}}\cos(\psi)A_{1,1}^t - \frac{i}{2\sqrt{5}}\sin(3\theta)B_{1,1}^t + \frac{3}{4\sqrt{14}}\sin(3\theta)\sin(2\psi)A_{2,0}^t \\
& + \frac{3i}{2\sqrt{21}}\sin(3\theta)\cos(2\psi)A_{2,1}^t + \frac{3}{2\sqrt{21}}\cos(3\theta)\cos(\psi)B_{2,1}^t + \frac{3}{4\sqrt{21}}\sin(3\theta)\sin(2\psi)A_{2,2}^t - \frac{3i}{2\sqrt{21}}\cos(3\theta)\sin(\psi)B_{2,2}^t \\
& + \frac{i\cos(\theta)}{2\sqrt{10}}[1 - 3\cos^2(\theta) - 10\cos^2(\psi) + 15\cos^2(\theta)\cos^2(\psi)]\sin(\psi)A_{3,0}^t - \frac{3\cos(\theta)}{2\sqrt{30}}[15\cos^2(\theta)\cos^2(\psi) - 10\cos^2(\psi) \\
& + 7 - 11\cos^2(\theta)]\cos(\psi)A_{3,1}^t - \frac{3i\sin(\theta)}{2\sqrt{30}}\{[5\cos^2(\psi) - 1]\cos^2(\theta) - 1\}B_{3,1}^t + \frac{3i\cos(\theta)}{2\sqrt{3}}[3\cos^2(\theta)\cos^2(\psi) - \cos(2\psi) \\
& - \cos^2(\theta)]\sin(\psi)A_{3,2}^t - \frac{\sqrt{3}}{8}[\sin(\theta) + \sin(3\theta)]\sin(2\psi)B_{3,2}^t - \frac{\cos(\theta)}{2\sqrt{2}}[3\cos^2(\theta)\cos^2(\psi) - 2\cos^2(\psi) - 3\cos^2(\theta) \\
& + 3]\cos(\psi)A_{3,3}^t - \frac{i\sin(\theta)}{2\sqrt{2}}[1 - 3\cos^2(\theta) + 3\cos^2(\theta)\cos^2(\psi)]B_{3,3}^t + \frac{5\sin(\theta)}{4\sqrt{70}}\{[7\cos^2(\psi) - 3]\cos^2(\theta) - 1\}\sin(2\psi)A_{4,0}^t \\
& + \frac{i}{2\sqrt{14}}\sin(\theta)\{[-27\cos^2(\psi) + 3 + 28\cos^4(\psi)]\cos^2(\theta) - \cos(2\psi)\}A_{4,1}^t + \frac{\cos(\theta)}{2\sqrt{14}}\{[7\cos^2(\psi) - 3]\cos^2(\theta) \\
& - 3\}\cos(\psi)B_{4,1}^t + \frac{\sin(\theta)}{2\sqrt{7}}\{[7\cos^2(\psi) - 4]\cos^2(\theta) + 1\}\sin(2\psi)A_{4,2}^t - \frac{i\cos(\theta)}{2\sqrt{7}}\{[7\cos^2(\psi) - 1]\cos^2(\theta) - 1\}\sin(\psi)B_{4,2}^t \\
& + \frac{i\sin(\theta)}{2\sqrt{2}}\{[1 - 5\cos^2(\psi) + 4\cos^4(\psi)]\cos^2(\theta) + \cos(2\psi)\}A_{4,3}^t + \frac{\cos(\theta)}{2\sqrt{2}}[1 - 3\sin^2(\psi)\cos^2(\theta)]\cos(\psi)B_{4,3}^t + \frac{\sin(\theta)}{4}[1 \\
& - \sin^2(\psi)\cos^2(\theta)]\sin(2\psi)A_{4,4}^t - \frac{i\cos(\theta)}{2}[1 - \sin^2(\psi)\cos^2(\theta)]\sin(\psi)B_{4,4}^t, \qquad \text{(E2)}
\end{aligned}
$$

$$F^{t(\mathrm{E2\text{-}E2})}_{\pi'\text{-}\pi} = \frac{\cos(4\theta)}{2\sqrt{5}}A^t_{0,0} - \frac{i\sin(4\theta)}{\sqrt{10}}\cos(\psi)A^t_{1,0} - \frac{\sin(4\theta)}{\sqrt{5}}\sin(\psi)A^t_{1,1} + \frac{\cos(4\theta)}{2\sqrt{14}}[3\cos^2(\psi)-1]A^t_{2,0} - \frac{3i}{2\sqrt{21}}\cos(4\theta)\sin(2\psi)A^t_{2,1}$$
$$- \frac{3\cos(4\theta)}{2\sqrt{21}}\sin^2(\psi)A^t_{2,2} - \frac{i\sin(4\theta)}{4\sqrt{10}}\cos(\psi)[5\cos^2(\psi)-3]A^t_{3,0} - \frac{3\sin(4\theta)}{4\sqrt{30}}\sin(\psi)[5\cos^2(\psi)-1]A^t_{3,1}$$
$$+ \frac{i\sqrt{3}}{4}\sin(4\theta)\sin^2(\psi)\cos(\psi)A^t_{3,2} + \frac{\sin(4\theta)}{4\sqrt{2}}\sin^3(\psi)A^t_{3,3} + \frac{\sqrt{70}}{16}\left[\frac{\cos(4\theta)}{35}\left\{\frac{3}{2} + \left[\frac{35}{2}\cos^2(\psi) - 15\right]\cos^2(\psi)\right\}\right.$$
$$\left. - \frac{1}{2}\sin^4(\psi)\right]A^t_{4,0} + \frac{7i}{8\sqrt{14}}\left\{\frac{\cos(4\theta)}{7}[3 - 7\cos^2(\psi)] - \sin^2(\psi)\right\}\sin(2\psi)A^t_{4,1} - \frac{1}{8\sqrt{7}}\{\cos(4\theta)[7\cos^2(\psi)-1] - 7$$
$$- 7\cos^2(\psi)\}\sin^2(\psi)A^t_{4,2} - \frac{i\sqrt{2}}{16}[\cos(4\theta)\cos^2(\psi) - \cos(4\theta) - \cos^2(\psi) - 3]\sin(2\psi)A^t_{4,3} + \frac{1}{16}[\cos(4\theta)\sin^4(\psi) - 1$$
$$- \cos^4(\psi) - 6\cos^2(\psi)]A^t_{4,4}. \tag{E3}$$

In Eq. (B1) $J^K_Q=(-1)^{K+Q}H^K_{-Q}$, where H^K_Q is found in Table IV of Ref. 6.

We note the following properties of the E2-E2 unit-cell structure factors. (a) $F^t_{\sigma'\text{-}\sigma}$ and $F^t_{\pi'\text{-}\pi}$ are functions of $A^t_{K,Q}$ only; (b) in $F^t_{\sigma'\text{-}\sigma}$ all contributions depend on 2θ whereas in $F^t_{\pi'\text{-}\pi}$ all contributions depend on 4θ; (c) $F^t_{\sigma'\text{-}\sigma}$ and $F^t_{\pi'\text{-}\pi}$ contain even and odd harmonics of ψ and a constant; (d) $F^t_{\pi'\text{-}\sigma}$ and $F^t_{\sigma'\text{-}\pi}$ have opposites signs to all $A^t_{K,Q}$ while all $B^t_{K,Q}$ are the same in the rotated channels, which is a rule shared with corresponding E1-E1 structure factors.

APPENDIX F: STRUCTURE FACTORS FOR NONCOLLINEAR CYCLOIDAL MODELS

We consider cycloidal structures traced out in the x-y, x-z, and y-z planes of right-handed orthonormal coordinates (x,y,z). The pitch is $1/(2n+1)$ and the fractional wave vector is $f/(2n+1)$ with integer n and f. For example, C-type reflections discussed in Sec. III C with a wave vector $\mathbf{q} \sim 0.28\mathbf{b}^*$ are simulated by $f=7$ and $n=12$ to a good approximation, whereas one could use $f=n=1$ as a crude approximation. Structures so defined are handed (chiral). The sense of hand is such that viewed down the axis normal to the plane rotation is counter clockwise (structurally right handed).

With our scheme of things, a multipole is replaced by a cycloidal structure factor C^K_Q calculated in a supercell with $(2n+1)$ elements. In general, the complex conjugate of C^K_Q is not equal to $(-1)^Q C^K_{-Q}$, unlike the multipole it replaces. Here we write expressions in terms of multipoles $\langle T^K_Q\rangle$ but they are equally valid for parity-odd multipoles because only proper rotations are employed.

Let $\phi=2\pi/(2n+1)$. The generic form of our cycloidal structure factor is,

$$C^K_Q = \sum_0^{2n}\frac{e^{im\phi f}}{2n+1}\langle T^K_Q\rangle_m = \frac{1}{2n+1}(\langle T^K_Q\rangle_0 + e^{i\phi f}\langle T^K_Q\rangle_1 + e^{2i\phi f}\langle T^K_Q\rangle_2 + \cdots + e^{2ni\phi f}\langle T^K_Q\rangle_{2n}), \tag{F1}$$

where $\langle T^K_Q\rangle_m$ stands for $\langle T^K_Q\rangle$ rotated in the plane of the cycloid through an angle $m\phi$.

For the x-y plane $\langle T^K_Q\rangle_m = e^{im\phi Q}\langle T^K_Q\rangle$, and one finds that C^K_Q is zero unless f and Q are specifically related, i.e., there is a selection rule on f and Q. With $\theta=\phi(f+Q)$ a simple calculation gives

$$C^K_Q = \frac{\langle T^K_Q\rangle}{2n+1}\left(\cos(n\theta) + \frac{\sin(n\theta)}{\tan(\theta/2)}\right) = \begin{cases} 0 & \text{if } (f+Q) \neq m'(2n+1) \\ \langle T^K_Q\rangle & \text{if } (f+Q) = m'(2n+1), \end{cases} \tag{F2}$$

where m' is an arbitrary integer (values of Q are limited by the triangle rule $-K \leq Q \leq K$). In this instance, complex conjugation satisfies $(C^K_Q)^* = (-1)^Q C^K_{-Q}$ but the relation does not hold for the x-z and y-z planes with rotation of multipoles around the y and x axes, respectively. We find

$$(2n+1)(C_Q^K \pm C_{-Q}^K) = [\langle T_Q^K\rangle \pm (-1)^Q \langle T_Q^K\rangle^*] + \sum_q [\langle T_q^K\rangle \pm (-1)^Q \langle T_q^K\rangle^*] \sum_{m=1}^{n} d_{Qq}^K(m\phi)\{\cos(m\phi f)[1+(-1)^{Q+q}] + i\,\sin(m\phi f)[1-(-1)^{Q+q}]\} \tag{F3}$$

for rotation in the x-z plane and,

$$(2n+1)(C_Q^K \pm C_{-Q}^K) = [\langle T_Q^K\rangle \pm (-1)^Q \langle T_Q^K\rangle^*] + 2\sum_{m=1}^{n} \sum_q d_{Qq}^K(m\phi)\cos(m\phi f)\cos\frac{(Q-q)\pi}{2}[\langle T_q^K\rangle \pm (-1)^Q \langle T_q^K\rangle^*] + 2\sum_{m=1}^{n} \sum_q d_{Qq}^K(m\phi)\sin(m\phi f)\sin\frac{(Q-q)\pi}{2}[\langle T_q^K\rangle \mp (-1)^Q \langle T_q^K\rangle^*] \tag{F4}$$

for rotation in the y-z plane. In Eqs. (F3) and (F4), $d_{Qq}^K(\psi)$ is a purely real element of the rotation matrix that also appears in Eq. (7). The sum on m ranges from $m=1$ to $m=n$, and $q=0, \pm 1, \pm 2$, etc. If the projection Q is restricted to either even or odd integer values, expressions (F3) and (F4) are purely real or purely imaginary. Such conditions on the projection might be imposed by the symmetry of the environment in which the reference ion is placed. However, in the general case, when Q takes both even and odd integer values, structure factors C_Q^K are complex quantities and $(C_Q^K)^* \neq (-1)^Q C_{-Q}^K$.

*scagnoli@esrf.eu

[1] D. Templeton and L. Templeton, Acta Crystallogr., Sect. A: Cryst. Phys., Diffr., Theor. Gen. Crystallogr. **38**, 62 (1982).
[2] K. D. Finkelstein, Q. Shen, and S. Shastri, Phys. Rev. Lett. **69**, 1612 (1992).
[3] V. Dmitrienko, Acta Crystallogr., Sect. A: Found Crystallogr. **39**, 29 (1983).
[4] P. Carra and B. T. Thole, Rev. Mod. Phys. **66**, 1509 (1994).
[5] V. Dmitrienko, K. Ishida, A. Kirfel, and E. N. Ovchinnikova, Acta Crystallogr., Sect. A: Found Crystallogr. **61**, 481 (2005).
[6] S. W. Lovesey, E. Balcar, K. S. Knight, and J. F. Rodriguez, Phys. Rep. **411**, 233 (2005).
[7] S. P. Collins, S. W. Lovesey, and E. Balcar, J. Phys.: Condens. Matter **19**, 213201 (2007).
[8] D. Templeton and L. Templeton, Acta Crystallogr., Sect. A: Found Crystallogr. **42**, 478 (1986).
[9] S. W. Lovesey, J. Fernández-Rodríguez, J. A. Blanco, and Y. Tanaka, Phys. Rev. B **75**, 054401 (2007).
[10] J. Blasco, C. Ritter, J. García, J. M. de Teresa, J. Pérez-Cacho, and M. R. Ibarra, Phys. Rev. B **62**, 5609 (2000).
[11] J.-S. Zhou and J. B. Goodenough, Phys. Rev. B **77**, 132104 (2008).
[12] I. Marri and P. Carra, Phys. Rev. B **69**, 113101 (2004).
[13] R. Kajimoto, H. Yoshizawa, H. Shintani, T. Kimura, and Y. Tokura, Phys. Rev. B **70**, 012401 (2004).
[14] M. Kenzelmann, A. B. Harris, S. Jonas, C. Broholm, J. Schefer, S. B. Kim, C. L. Zhang, S.-W. Cheong, O. P. Vajk, and J. W. Lynn, Phys. Rev. Lett. **95**, 087206 (2005).
[15] D. Senff, P. Link, K. Hradil, A. Hiess, L. P. Regnault, Y. Sidis, N. Aliouane, D. N. Argyriou, and M. Braden, Phys. Rev. Lett. **98**, 137206 (2007).
[16] O. Prokhnenko, R. Feyerherm, M. Mostovoy, N. Aliouane, E. Dudzik, A. U. B. Wolter, A. Maljuk, and D. N. Argyriou, Phys. Rev. Lett. **99**, 177206 (2007).
[17] T. Kimura, T. Goto, H. Shintani, K. Ishizaka, T. Arima, and Y. Tokura, Nature (London) **426**, 55 (2003).
[18] D. Meier, N. Aliouane, D. N. Argyriou, J. A. Mydosh, and T. Lorenz, New J. Phys. **9**, 100 (2007).
[19] M. Fiebig, J. Phys. D **38**, R123 (2005).
[20] D. Mannix, D. F. McMorrow, R. A. Ewings, A. T. Boothroyd, D. Prabhakaran, Y. Joly, B. Janousova, C. Mazzoli, L. Paolasini, and S. B. Wilkins, Phys. Rev. B **76**, 184420 (2007).
[21] J. Voigt, J. Persson, J. W. Kim, G. Bihlmayer, and T. Brückel, Phys. Rev. B **76**, 104431 (2007).
[22] S. W. Lovesey, K. S. Knight, and E. Balcar, J. Phys.: Condens. Matter **19**, 376205 (2007).
[23] D. A. Varshalovic, A. N. Moskalev, and V. K. Khersonskii, *Quantum Theory of Angular Momentum* (World Scientific, Singapore, 1988).